


Article

Regulation of Macrophage Behavior by Chitosan Scaffolds with Different Elastic Modulus

Jiawei Xu^{1,2,3}, Wenchao Guan^{1,2,3}, Yan Kong^{1,2,3}, Fang Liu^{1,2,3}, Yahong Zhao^{1,2,3}, Guicai Li^{1,2,3,*} 
and Yumin Yang^{1,2,3,*}

¹ Key Laboratory of Neuroregeneration of Jiangsu and Ministry of Education, Nantong University, Nantong 226001, China

² Co-Innovation Center of Neuroregeneration, Nantong University, Nantong 226001, China

³ NMPA Key Lab for Research and Evaluation of Tissue Engineering Technology Products, Nantong University, Nantong 226001, China

* Correspondence: gcli1981@ntu.edu.cn (G.L.); yangym@ntu.edu.cn (Y.Y.)

Abstract: Increasing evidence shows that the physical properties of biomaterials play an important role in regulating cell behavior and function, especially the mechanical properties of biomaterials. Macrophages can also be multidirectionally regulated by mechanical factors in the microenvironment, which simultaneously mediate biomaterials response that triggered by foreign body reactions (FBR). However, how the stiffness of biomaterials regulates macrophages and the underlying mechanisms are still not well understood. Our study demonstrates that chitosan freeze-dried scaffolds with different elastic modulus can modulate the proliferative capacity, growth morphology and polarization behavior of macrophages. The compression tests and morphology observation confirmed that the prepared lyophilized chitosan scaffolds possessed varied stiffness. The fluorescence staining experiments showed that the RAW macrophage cell lines exhibited differences in proliferation and morphology on the freeze-dried scaffolds with different stiffness. Macrophages in the 5% group (elastic modulus of 106.7 kPa) had the largest number and mean cell area. Furthermore, ELISA and qPCR results illustrated that macrophage polarization towards the M1/M2 phenotype was strongly influenced by the stiffness of the lyophilized scaffolds. The study may provide new insights and references for designing the elastic moduli of biomaterials for regulating immune responsiveness.

Keywords: chitosan; lyophilized scaffolds; elasticity; macrophages; polarization



Citation: Xu, J.; Guan, W.; Kong, Y.; Liu, F.; Zhao, Y.; Li, G.; Yang, Y. Regulation of Macrophage Behavior by Chitosan Scaffolds with Different Elastic Modulus. *Coatings* **2022**, *12*, 1742. <https://doi.org/10.3390/coatings12111742>

Academic Editor: Devis Bellucci

Received: 13 October 2022

Accepted: 11 November 2022

Published: 14 November 2022

Publisher's Note: MDPI stays neutral with regard to jurisdictional claims in published maps and institutional affiliations.



Copyright: © 2022 by the authors. Licensee MDPI, Basel, Switzerland. This article is an open access article distributed under the terms and conditions of the Creative Commons Attribution (CC BY) license (<https://creativecommons.org/licenses/by/4.0/>).

1. Introduction

The biocompatibility of material is one of the important indicators of the tissue repair effect. Once the material is implanted in the body, it will cause a series of cellular activities, initiate the body's immune response and lead to the formation of inflammation [1,2]. Firstly, the implanted material rapidly adsorbs proteins (such as fibrinogen, albumin and immunoglobulin G) in the blood, forming a protein coating on the surface of the material [3]. Among them, the adsorbed fibrinogen stimulates mast cells to release histamine and promotes the recruitment of macrophages to the implantation site, causing an acute inflammatory response [4]. In addition, the newly formed protein interface activates the complement system, platelets and coagulation proteins, etc., and forms blood clots around the implant, which further activate and recruit macrophages and exacerbate the inflammatory response [5,6]. Macrophages are the main phagocytic cells in the human immune system which are derived from the monocytes in bone marrow [7]. They are white blood cells with a wide range of guards in the human body. In the process of wound repair in the body, macrophages mainly play two roles. On the one hand, macrophages secrete a variety of biologically active substances and enzymes, such as polypeptide transforming growth factor and interleukin, to promote wound repair in the process of body injury. On the other hand, macrophages play a role in phagocytosis to remove tissue, cell debris and pathogens

from the damaged body, which promotes the repair and healing of damage in the inflammatory stage. Macrophages are divided into many phenotypes, and different phenotypes have different or even opposite effects. Classically activated macrophages are proinflammatory phenotypes (M1 macrophages) that secrete the additional proinflammatory cytokines TNF- α , IL-1 β and nitric oxide synthase (iNOS) after chemokine recruitment to kill bacteria and other microorganisms [8–10], while M2 macrophages do not deliver antigens to T cells. They are activated alternately by IL-4 and IL-13 and secrete the anti-inflammatory factors IL-4 and IL-10 which have anti-inflammatory effects [11–13]. At the same time, M2 macrophages secrete the vascular endothelial growth factor (VEGF) and transforming growth factor β (TGF- β), etc., to promote the reconstruction of the extracellular matrix and tissue regeneration [13,14]. Although it is too simple to classify macrophages into M1/M2 phenotypes which cannot truly express the dynamic process of macrophages in vivo, this classification allows us to quickly understand the functions and changes in macrophages in an in vivo niche [15]. Therefore, an appropriate ratio of M1 and M2 macrophages is beneficial to obtain an appropriate immune response from the biomaterials, which not only resists the risk of infection but also promotes tissue repair and regeneration.

Mechanical cues, including physical and chemical properties, affect cell adhesion, migration, proliferation and function, such as the material mechanical properties, biodegradability, magnetic properties, surface topography, etc. [16–19]. Among them, the mechanical properties are a factor that cannot be ignored in the design of biomaterials, which refers to the performance of materials when bearing various external loads (tensile, compressive, bending, torsion, impact, alternating stress) under different environments (temperature, medium, humidity) [20]. The elastic modulus is an index of particular concern in the mechanical properties in the process of the tissue engineering of biomaterials. When a cell is in contact with a material, the elastic deformation of the material imparts stress to the cell, causing the cell to deform, thus changing the cytoskeleton and transmitting biological signals to the genetic material, ultimately presenting different biological effects. In recent years, many studies have confirmed the effect of material elasticity on cell and tissue regeneration [21,22]. Stem cells, as a kind of cell with strong proliferation and differentiation ability, have great differences in their differentiation behavior with the change in the elasticity of the extracellular matrix. [23]. Oh et al. successfully prepared a PVA/HA matrix with a gradient elastic modulus and confirmed that human bone marrow mesenchymal stem cells tend to differentiate into different types of cells on different elastic matrices through in vitro cell culture experiments (about 20 kPa for nerve cells, about 40 kPa for muscle cells, about 80 kPa for chondrocytes and about 190 kPa for osteoblasts) [24]. Although macrophages do not possess a differentiation capacity, they show diversity in the elasticity of the matrix. The elasticity of the substrate leads to the reorganization of the cytoskeleton through contact, spreading and adhesion which accounts for the differences in morphology and function [25,26]. Studies have shown that macrophages display different surface clearance and phagocytosis capabilities for submicron particles with different stiffness [27]. In addition, macrophages are more prone to polarization towards the M1 type in the condition of a high stiffness matrix [25]. However, how biomaterials with different elastic modulus affect the morphology and function of macrophages and the underlying mechanisms is rarely studied.

There are many mature biomaterial mechanical property control systems at present. The elastic modulus of material can be adjusted to the value we desire by changing the ratio of the crosslinking monomers or the degree of the crosslinking [28,29]. For example, the mechanical properties of hydrogels can be easily changed using different types and concentrations of crosslinking agents [30]. Chitosan is one of the biomaterials with safe and excellent biological properties, which is approved by the FDA and widely used in the field of tissue repair and regeneration [31]. It is the only natural cationic polysaccharide found in nature and the most abundant polymer, second only to cellulose [32]. Chitosan is obtained by the partial deacetylation of chitin and shows good biocompatibility, biodegradability, non-antigenicity and antibacterial activity [33–39]. Chitosan is not bioactive by itself;

however, blending it with bioactive ceramic, bioglasses, other bioactive polymers such as gelatin and the loading of bioactive molecules can make it the ideal composite for different tissue engineering applications [40,41]. It has been studied that the elastic modulus of chitosan gel can be altered by adjusting the degree of acetylation [42]. There have been studies involving chitosan scaffolds or gels with different mechanical properties for regulating cell growth, but there are few reports on their effects on macrophages.

In this study, chitosan scaffolds with different elasticity were prepared by freeze-drying chitosan solutions of different concentrations. The rheological properties, elastic modulus, surface morphology, water uptake and wettability of the scaffolds were measured to analyze the differences in the physicochemical properties of the scaffolds with different elastic modulus. Then, the morphological changes, polarization directions and cell viability differences of the macrophages on the chitosan scaffolds with different elastic modulus were observed using *in vitro* cell culture experiments. Following a morphological analysis, the proteins and molecules of the macrophages related to the polarization behavior were determined and analyzed using an enzyme-linked immunosorbent assay (ELISA) experiment, Western blot and a qPCR experiment. We tried to elucidate the differential growth behavior of the macrophages on the chitosan scaffolds with different elastic modulus as well as the intrinsic mechanism of the phenomenon through this experiment.

2. Materials and Methods

2.1. Materials and Reagents

Pharmaceutical grade chitosan (Xingcheng, Nangtong, China) was obtained from Alaskan snow crab with a deacetylation degree of about 90% and a viscosity of about 60cP. Then, chitosan was dissolved in 2% (*v/v*) acetic acid solution which was obtained from Honeywell. RAW 264.7 was obtained from Cell Bank of Chinese Academy of Sciences. Mouse IL-6 ELISA Kit and Mouse IL-10 ELISA Kit were both obtained from Linktech in China. In addition, 1640 medium, fetal bovine serum and penicillin–streptomycin were all obtained from Gibco. Phalloidin-iFluor 488 Reagent and DAPI were both obtained from Abcam.

2.2. Preparation of Freeze-Dried Chitosan Scaffolds with Different Elasticity

Different weights of chitosan powder were dissolved in 2% (*v/v*) acetic acid solution and evenly stirred to prepare chitosan solutions with different concentrations (1%, 3%, 5% and 7%). Chitosan solutions of different concentrations were added to a 24-well plate at 500 μ L per well with 1 mL injections and were left for 24 h to eliminate air bubbles. After the samples were frozen at -20 °C for 12 h, they were placed in a freeze dryer (Bilang, Shanghai, China) for 24 h. Then, the freeze-dried scaffolds were soaked with 4% (*w/v*) NaOH solution for 4 h at a volume ratio of 1:10 to neutralize the acetic acid in the scaffolds. The samples were then washed with distilled water until neutral so that the unreacted NaOH was completely removed. Finally, freeze-dried chitosan scaffolds with different elasticity were obtained (Figure 1). Then, the scaffolds were immersed in PBS at 37 °C for reservation for the following experiments.

2.3. Characterization of Freeze-Dried Chitosan Scaffolds with Different Elasticity

2.3.1. The Rheological Analysis

First, 1 mL of 1%, 3%, 5% and 7% chitosan solutions were placed on the rheometer sample stage (Thermo Fisher Scientific, RheoWin MARS 40, Waltham, MA, USA) at room temperature, and the shear rate was set from 0 to 50 (1/s) in order that changes in viscosity of chitosan solution with the shear rate increasing could be observed.

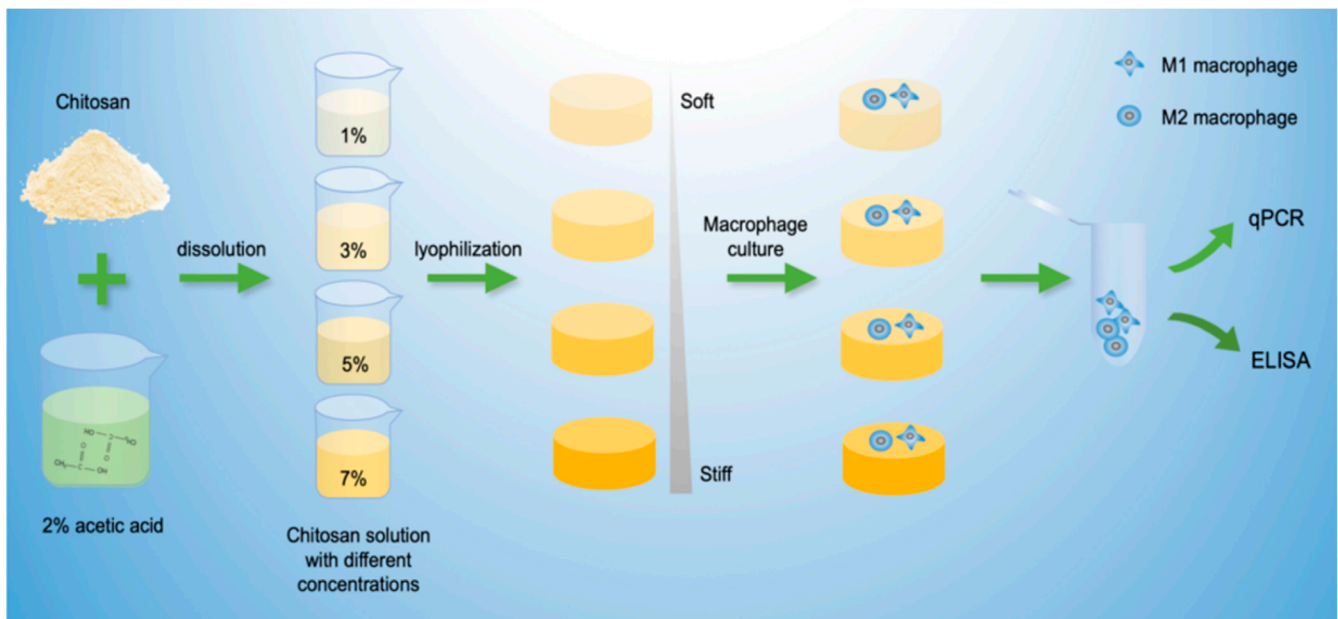


Figure 1. Schematic diagram of preparation of freeze-dried scaffolds with different elastic chitosan and study on the regulation of elasticity on macrophages.

2.3.2. Modulus of Elasticity

The freeze-dried chitosan scaffolds with diameter of 10 mm and thickness of 2 mm were placed on the sample stage of the universal electronic stretching machine (Fengtuo, Shanghai, China), and the program was set under compression mode with loading force of 100 N. The parameters of the stretching machine were set to measure the stress–strain curve of the samples. The elasticity modulus of the samples was obtained by calculating the slope of the stress–strain curve in elastic deformation stage.

2.3.3. Morphology

Next, the chitosan scaffolds were freeze-dried for 48 h in order to remove water. The secondary freeze-dried chitosan scaffolds were fixed on the stage with conductive glue, and a gold layer was sprayed on the surface of the sample. Then, scanning electron microscope (SEM, JEOL, Tokyo, Japan) was used to observe and photograph the morphology of freeze-dried chitosan scaffolds with different concentrations at high magnification.

2.3.4. Water Uptake

The freeze-dried chitosan scaffolds with diameter of 10 mm and thickness of 2 mm were freeze-dried on filter paper for a second time to remove water. Three parallel samples were taken for each concentration. The weights of the samples under the freeze-dried state were recorded as W_0 , and the weights of the freeze-dried scaffolds after being soaked in water for 5, 10, 20 and 30 min, and 1, 2, 4 and 8 h were recorded as W_1 . The formula for calculating water uptake is as follows:

$$\text{Water uptake (\%)} = (W_1 - W_0) / W_0 \times 100$$

2.3.5. Contact Angle

Excess water of the samples was absorbed with filter paper. Then, the samples were placed on the sample stage of the contact angle measuring instrument (JY-PHA, Chengdejinhe, Chengde, China), and the microinjector with the same scale was rotated to make water droplets of the same volume. The contact angle was measured when the droplets dropped onto the surface of the scaffolds.

2.4. Biological Evaluation of Freeze-Dried Chitosan Scaffolds with Different Elasticity

2.4.1. Sterilization of Materials

The samples were soaked in 75% (*v/v*) ethanol for 30 min and then irradiated with a UV lamp for 30 min. Afterwards, the samples were washed with sterile water three times and rinsed with 1640 medium for use. The sterilized materials were subsequently used in cell culture experiments.

2.4.2. Cell Viability Assay

The freeze-dried scaffolds with different concentrations of chitosan were extracted with 1640 medium for 24 h at a volume ratio of 1:10 to prepare a complete medium (containing 10% fetal bovine serum, 1% penicillin–streptomycin). Mouse mononuclear macrophage leukemia cells (RAW 264.7) were seeded at 3000 cells per well in 96-well plates. After 4 h, the original medium was trashed, and 200 μ L of complete medium prepared with chitosan extracts of different concentrations and normal medium as controls were added to 96-well plates. After incubation for 1 and 3 d, the culture medium in the well plates was discarded, and 200 μ L of Cell Counting Kit-8 (CKK-8) solution was added to the experimental wells and blank wells and incubated in the dark for 4 h [43,44]. Then, the absorbance at 450 nm was measured with a microplate reader (Bio-Tek, Winooski, VT, USA), and the cell viability was calculated as follows:

$$\text{Cell viability (\%)} = [\text{OD}(\text{experiment}) - \text{OD}(\text{blank})] / [\text{OD}(\text{control}) - \text{OD}(\text{blank})] \times 100$$

2.4.3. Cell Fluorescence Staining

The RAW 264.7 cells were seeded on the sterilized scaffolds in 24-well plate at the number of 50,000 per well. After culturing for 1 and 3 days, the medium was discarded, and 500 μ L of 4% paraformaldehyde was added to each well to fix cells for 1 h. Then, the paraformaldehyde was discarded, and the materials were washed three times with phosphate buffered saline (PBS). Next, 500 μ L of immunofluorescence blocking solution was added to each well to block for 2 h at room temperature. Then, 200 μ L of Phalloidin-iFluor 488 Reagent (Abcam, Cambridge, UK) was added at 1/1000 dilution in PBS to each well and incubated at room temperature for 90 min [45]. The materials were washed three times with PBS. Subsequently, 200 μ L of DAPI (Sigma, St. Louis, MO, USA) at 1/1000 dilution in PBS was added to each well and incubated at room temperature for 10 min. The materials were washed three times with PBS, and 500 μ L of fluorescent mounting fluid was added per well. Then, the cells were observed and photographed under a confocal microscope (SP5; Leica, Heerbrugg, Germany).

2.4.4. ELISA

The RAW 264.7 cells were seeded on the sterilized 24-well plate at the number of 50,000 per well. Subsequently, the cell culture medium was collected after culturing for 1 and 3 days. Interleukin-6 (IL-6) and interleukin-10 (IL-10) in the culture medium were extracted and quantified according to the steps of the IL-6 and IL-10 ELISA kit (Multiscience, Hangzhou, China). The absorbance at 450 nm and 570 nm was measured using a microplate reader to determine the concentration of IL-6 and IL-10 in the culture medium.

2.4.5. Real-Time Polymerase Chain Reaction (RT-PCR) Analysis

The RAW 264.7 cells were seeded on sterilized material in a 24-well plate at a density of 100,000 per well. Then, the medium was discarded after 1 and 3 days, and 250 μ L of TRI Reagent (Sigma, St. Louis, MO, USA) was added to each well to extract RNA. First strand complementary DNA (cDNA) was synthesized by reverse transcription of extracted RNA using PrimeScript RT reagent kit (Takara, Tokyo, Japan). Interleukin-1 (IL-1) was evaluated with GAPDH used as the house keeping gene. The relative expression level for each gene (fold change) was calculated using Livak method with $2^{-\Delta\Delta C_t}$ and normalized to that of the

reference gene GAPDH. The primers for RT-PCR are listed in Table 1. Relative expression was quantified using the comparative threshold method.

Table 1. Primer sequences.

Gene	Forward Primer Sequences (5'-3')	Reverse Primer Sequences (3'-5')
GAPDH	GCTCAGGCCTCTGCGCCCT	CCTACTCTCTTGAATACC
IL-1	GAAATGCCACCTTTTGACAGG	TGGATGCTCTCATCAGGACAG

2.5. Data Analysis

All data are expressed as means \pm SEM. The *t*-test and one-way analysis of variance (ANOVA) were used to statistically analyze the data via GraphPad Prism 8. A probability (*p*) value less than 0.05 ($p < 0.05$) was considered as significant difference.

3. Results

3.1. The Rheological Analysis

Chitosan is a water-insoluble powder that can only be dissolved in organic or inorganic acids. Therefore, a 2% acetic acid solution was used to dissolve chitosan in this experiment, and the solutions with a chitosan concentration of 1%, 3%, 5% and 7% were successfully prepared. The rheological properties of the solutions also changed with the increase in the chitosan content. The viscosity of the chitosan solution was characterized using a rheometer (Figure 2). In the 1% and 3% groups, the viscosity of the solution hardly changed with the change in the shear rate (Figure 2a,b). Therefore, the viscosity of these two groups was a constant, and the solution viscosity of the 1% group and the 3% group was about 0.47 and 1.05 Pas. In the 5% and 7% groups, the viscosity of the solution significantly decreased with the increase in the shear rate which resulted from the fact that the viscosity of the solution increased with the increased content of chitosan, and the solution gradually became a non-Newtonian fluid whose viscosity was no longer a constant which meant the viscosity changed with the change in the shear rate (Figure 2c,d). However, under the same shear rate of 40 (1/s), the solution viscosity of the 5% and 7% groups was 6.78 and 22.12 Pas, respectively. Notably, the solution viscosity of the 7% group was the highest among all the groups. In general, the viscosity of the chitosan acetate solution increased with the increase in the chitosan concentration.

3.2. Modulus of Elasticity

The freeze-dried scaffolds prepared with various concentrations of chitosan solutions had different internal structures as a function of the volume ratios of chitosan and water. The internal structure of the scaffolds was directly related to the elastic modulus. The stress–strain curves of the different experimental groups in the elastic deformation stage showed that the freeze-dried scaffolds could withstand greater stress within the same strain range, which indicated that the scaffolds had a higher elastic modulus as the concentration of chitosan increased (Figure 3a). The slope of the stress–strain curves in the elastic deformation stage was calculated as the elastic modulus of the freeze-dried chitosan scaffolds (Figure 3b). The average elastic modulus of the 1%, 3%, 5% and 7% groups was 5.5, 40, 107 and 223 kPa, respectively. Therefore, the freeze-dried chitosan scaffolds with different concentrations exhibited various elastic properties and provided elastic reaction forces to the cells, which laid a foundation for the subsequent study of the effects of the elasticity of scaffolds on cell behavior and function.

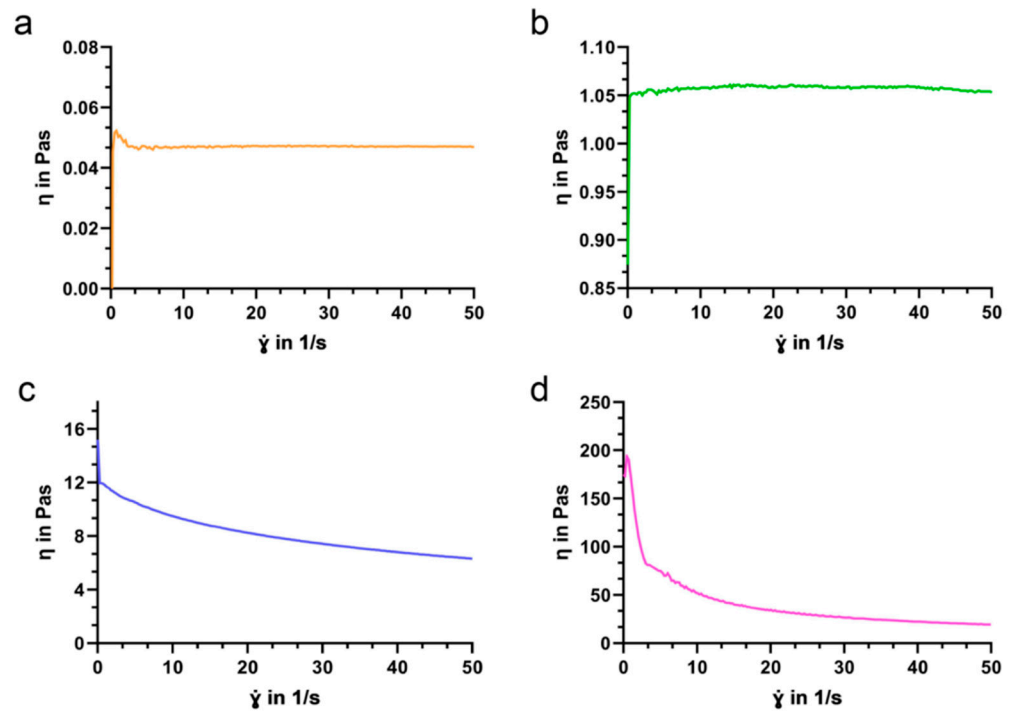


Figure 2. Rheological properties of chitosan solutions with different concentrations. (a–d) Viscosity–shear rate curve of chitosan solution with different concentrations. (a) 1%, (b) 3%, (c) 5%, (d) 7%.

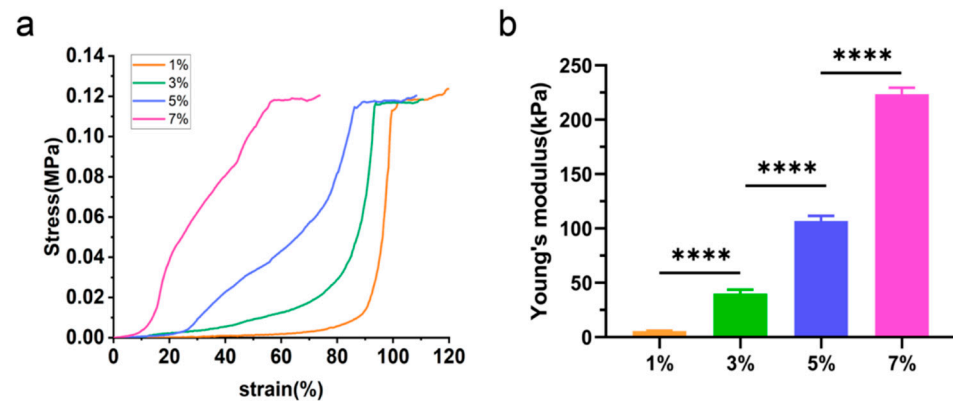


Figure 3. Stress–strain curves (a) and elastic modulus statistics (b) of freeze-dried chitosan scaffolds with different concentrations, $n = 6$, **** $p < 0.0001$.

3.3. Morphology of Freeze-Dried Scaffolds with Different Concentrations of Chitosan

Freeze-dried scaffolds are loose porous scaffolds prepared by directly subliming the water in them in a low-temperature vacuum environment after liquid freezing. The chitosan scaffolds with different concentrations have different microstructures due to their different water content. The surface and internal morphology of the freeze-dried scaffolds were observed using scanning electron microscopy (SEM) in order to explore the differences in the internal structure of the freeze-dried scaffolds (Figure 4a). The SEM images show that the chitosan freeze-dried scaffolds formed a uniform and dense pore structure inside, which satisfied the needs of the nutrient supply and material exchange for the cells. In addition, the pore size gradually became smaller, and the pore structure became more compact with the increase in the chitosan concentration (Figure 4b). The average pore size of 1%, 3%, 5% and 7% groups was 182, 148, 103 and 71 μm , respectively. The difference in the internal pore size and porosity results in the changes in the elastic modulus of the lyophilized scaffolds, which provides different sizes of support force for the macrophages.

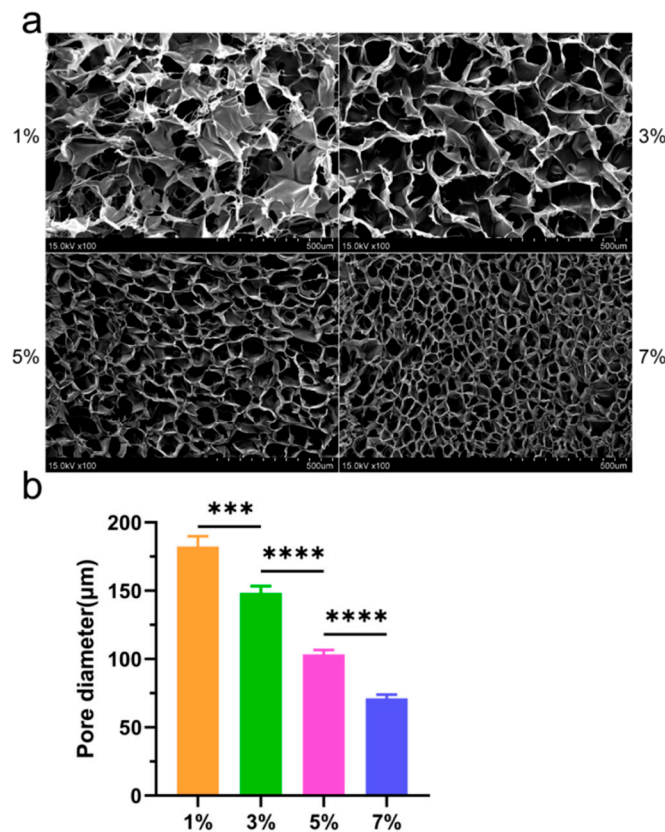


Figure 4. Cross-sectional SEM (a) and pore size statistics (b) of freeze-dried chitosan scaffolds at different concentrations, $n = 30$, *** $p < 0.001$, **** $p < 0.0001$.

3.4. Water Uptake of Freeze-Dried Scaffolds with Different Concentrations of Chitosan

The change in the internal pore size and porosity in the material will directly lead to the variation of the water uptake of the material. All freeze-dried scaffolds reached a water-saturated state after being soaked in water for ten minutes, indicating that the freeze-dried scaffolds possessed a sufficiently porous structure to provide nutrient support and substance exchange for the cells rapidly (Figure 5a). The quantitative statistics of the water uptake rate showed that the 1% group absorbed the most water and had the strongest water holding capacity under the same conditions (Figure 5b) due to its loose pore structure. The average water uptake of 1%, 3%, 5% and 7% was 3032%, 1836%, 775% and 634%, respectively, which was consistent with the previous analysis of the internal structure of lyophilized scaffolds.

3.5. Contact Angle of Freeze-Dried Scaffolds with Different Concentrations of Chitosan

The hydrophilicity of materials is one of the important aspects for the biological evaluation of biomedical materials. An appropriate surface hydrophilicity is beneficial for cell adhesion and migration. The contact angle is strong evidence that indicates the hydrophilicity status of the material. The surface contact angles of lyophilized chitosan scaffolds were measured and quantitatively analyzed in Figure 6, and the results indicate that there was no significant difference in the contact angles among the four experimental groups. Therefore, the different concentrations of chitosan in each experimental group did not affect the surface hydrophilicity of the freeze-dried scaffolds. The contact angles for all groups were in the range from 30° to 40°, confirming that the hydrophilicity may provide good interface conditions for cell adhesion and migration (Figure 6b).

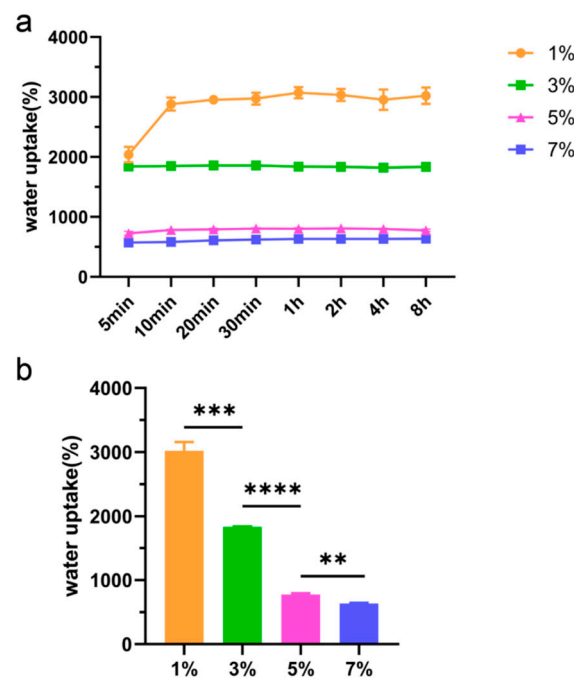


Figure 5. (a) Variation curve of water uptake rate of freeze-dried chitosan scaffolds with different concentrations over time, $n = 3$; (b) Statistical chart of water uptake rate after water saturation of freeze-dried scaffolds with different concentrations of chitosan, $n = 3$, ** $p < 0.01$, *** $p < 0.001$, **** $p < 0.0001$.

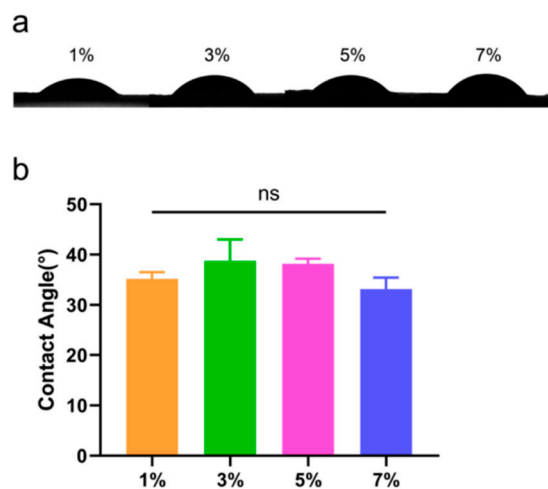


Figure 6. Hydrophilic analysis of different elastic chitosan lyophilized scaffolds. (a) Contact angle images of different elastic freeze-dried chitosan scaffolds; (b) Quantitative analysis of contact angles of different elastic freeze-dried chitosan scaffolds, $n = 6$, ns represents $p > 0.05$.

3.6. Cell Viability Assay

The freeze-dried chitosan scaffolds with various concentrations of chitosan are not only different in their physical properties but may also release soluble components into the medium which affects cell viability. Thence, the extract of the scaffolds was prepared to culture RAW cells. The CCK-8 results in Figure 7a show that there was no significant difference in the cell viability among the experimental groups at 1 or 3 days, respectively. Meanwhile the RAW cells stained with toluidine blue O (TBO) exhibited similar shapes and quantities in different groups at 1 or 3 days, respectively (Figure 7b). On the first day, most cells maintained a round shape, and the number of cells was low. By the third day, the number of cells expanded to a larger scale, and some cells became polarized with individual cells

sticking out with distinct protrusions. Regardless of day 1 or 3, the cells exhibited similar cell numbers and cell morphology in the experimental groups. Therefore, the lysates of the different concentrations of the lyophilized chitosan scaffolds in the medium did not show a significant effect on cell viability and morphology. The cell viability of all experimental groups could reach more than 70% compared with the control group, indicating that the prepared chitosan scaffolds in all groups have an excellent biocompatibility.

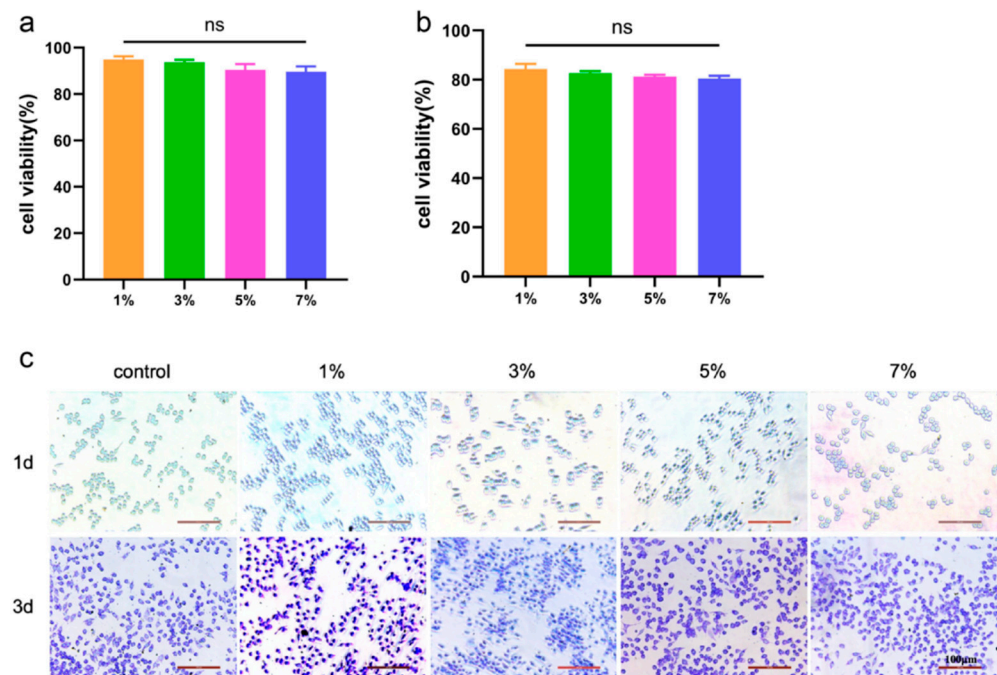


Figure 7. Effect of chitosan concentration on cell viability. RAW264.7 cells were cultured with different concentrations of chitosan freeze-dried scaffold extract, and the cell viability was measured using CCK-8 method at 1d (a) and 3d (b), $n = 8$, ns represents $p > 0.05$. Then, RAW264.7 cells were stained with TBO (c).

3.7. Cell Morphology

Macrophages are myeloid cells involved in the innate immune response, originating from monocyte precursors in the blood and play a key role in tissue homeostasis under normal physiological conditions as well as after tissue injury. Phagocytosis, exogenous antigen presentation and immune regulation through cytokine and growth factor secretion are its three key features. The microenvironment where macrophages are located is vital for their proliferation and migration. The chitosan freeze-dried scaffolds provide different specifications of support for the macrophages growing on the surface due to their different porosity to regulate the behavior and function of the macrophages.

On the first day of culture, the macrophages showed a differential affinity for different groups of materials (Figure 8a). The number of cells in the 5% group was significantly larger than the other three groups, while the number of cells in the 1% group was the smallest. In addition, cells in the 5% group grew in small flakes, close to the state of the cells in a Petri dish. Most of the cells in the 1% group independently grew and did not touch each other. On the third day, the cells in each group increased, and the spreading area of the cells enlarged. A few RAW cells showed obvious polarization behavior with stretching-out protrusions. Among them, the 5% group had the largest number of cells and the largest average area of cells (Figure 8b). In addition, a lot of the cells spread out in irregular shapes. Although the number of cells was more than that in day 1 in the 1% group, it was the least among the four groups, and most of the cells were spherical. Interestingly, as the chitosan concentration increased, the number and area of RAW cells decreased in the 7% group. The RAW cells showed the best proliferation and migration ability in the 5%

group, and the number and volume of cells were also the largest, while, vice versa, the 1% group was the worst.

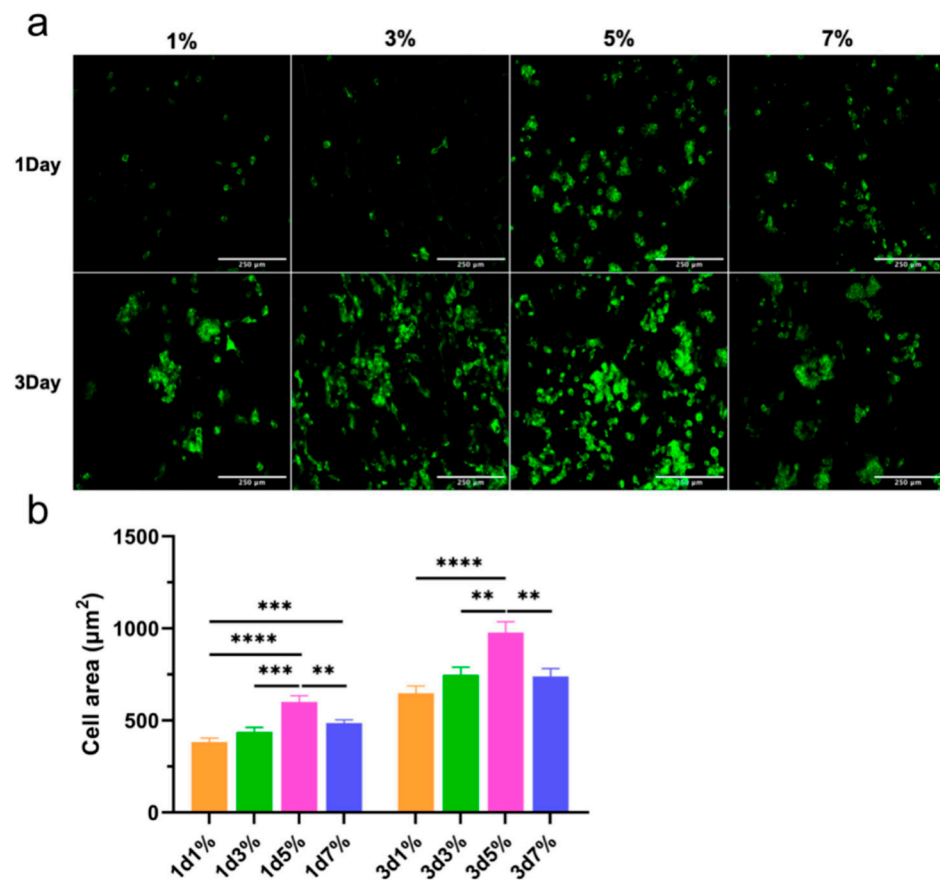


Figure 8. (a) RAW264.7 cells were cultured on different concentrations of chitosan freeze-dried scaffolds and stained with phalloidin. (b) Quantitative statistics of cell area, $n = 30$, ** $p < 0.01$, *** $p < 0.001$, **** $p < 0.0001$.

3.8. Pro- or Anti-Inflammatory Factors Secreted by Cells

The activation of macrophages plays a crucial role in tissue homeostasis as well as in inflammation and disease progression [46]. Macrophages can change their phenotype in response to many different stimuli, which is dynamic. In general, macrophages can be divided into classically activated M1 macrophages and alternatively induced M2 macrophages according to their function and activation. In the early stage of inflammation, classically activated M1 macrophages secrete factors, such as IL-6, which play a pro-inflammatory role. In the late stage of inflammation, alternately activated M2 macrophages secrete factors, such as IL-10, which play an anti-inflammatory role. The ELISA results show that the concentration of IL-6 decreased with the increasing stiffness of the lyophilized scaffolds on the first day. On the third day, the expression of IL-6 in the 1% group was still the highest, while it was the lowest in the 5% group (Figure 9a). The concentration of IL-6 in each group gradually increased over time. The concentration of IL-10 was generally lower than that of IL-6, and the overall trend was the opposite to that of IL-6. The 5% group had the highest IL-10 concentration on both the first and third days. When the concentration of chitosan was 1%–5%, the concentration of IL-10 increased with the elevation in the hardness of the freeze-dried scaffolds; when the concentration of chitosan was 5%–7%, the concentration of IL-10 decreased with the elevation in the hardness of the freeze-dried scaffolds (Figure 9b). Hence, the RAW cells have different polarization trends on the lyophilized scaffolds with different elasticity.

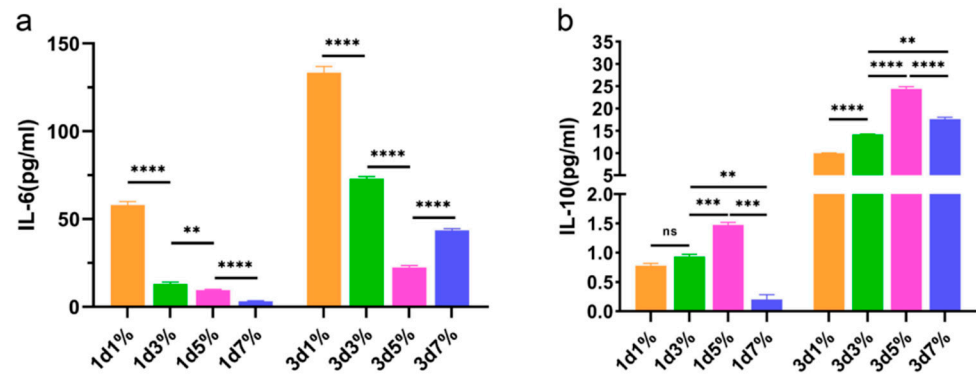


Figure 9. Concentrations of IL-6 (a) and IL-10 (b) in medium of RAW cells cultured on scaffolds at 1 and 3 days tested using ELISA, $n = 3$, ** $p < 0.01$, *** $p < 0.001$, **** $p < 0.0001$.

3.9. Gene Expression

Next, we verified the typing of the RAW macrophages in each group at the genetic level. The results of the qPCR experiment show that no matter whether it was the first or third day, the expression level of the marker IL-1 of the M1 macrophages had a gradually decreasing trend in the 1%, 3% and 5% groups, while it showed an upward trend in the 5% and 7% groups (Figure 10). The experimental results of the qPCR and ELISA show the same trend, as the IL-6 secreted by the M1 phenotype was also much higher than the IL-10 secreted by the M2 phenotype measured using the ELISA. Therefore, the regulation rules of the different elastic chitosan freeze-dried scaffolds on the RAW macrophages were further elaborated.

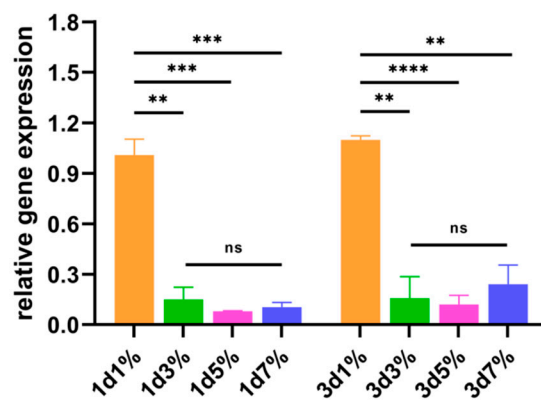


Figure 10. Real-time PCR analysis of the gene expression of the IL-1, $n = 3$, ns represents $p > 0.05$, ** $p < 0.01$, *** $p < 0.001$, **** $p < 0.0001$.

4. Discussion

The physical properties of biomaterials are increasingly becoming one of the important factors to consider when designing implants [47,48]. Cells are highly plastic, so the microenvironment created by the mechanical properties of the implant, especially the elasticity, has a profound influence on cell growth and development. Simultaneously, macrophages, as key immune cells that mediate FBR, can respond to the cellular microenvironment created by the materials and produce different degrees of inflammatory responses to the M1/M2 macrophages' polarization. The activity of macrophages against different biomaterials yields different biocompatibility outcomes. Our study intended to construct chitosan freeze-dried scaffolds with different elasticity to study the effects of biomaterials with different interface elasticity on the behavior and function of macrophages. To sum up, chitosan freeze-dried scaffolds can stimulate RAW cells to polarize in the M1/M2 direction, and the amount of polarization to the M1 type was greater than that of the M2 type. In the lower hardness range, the greater the elastic modulus of the material, the smaller the ratio of cells

polarized to the M1 type and the greater the ratio of polarization to the M2 type. Conversely, in the higher hardness range, the ratio of cells polarized to the M1 type increased, while the ratio of cells polarized to the M2 type decreased.

We have built a kind of material system with a controllable elastic modulus based on chitosan because of the excellent biological properties of chitosan [35–39,49]. As a naturally occurring polysaccharide, chitosan has excellent biocompatibility and antibacterial properties and is also one of the FDA-approved biomaterials [31]. Thus, when we focus on the effects of the physical properties of the material on the cells, the cells are in a relatively healthy state so that the differences in cell behavior and function will not be masked. The CCK8 results also prove that there was no significant difference in the cell viability and proliferation ability of the leaching solution of the lyophilized scaffolds. Due to the different ratios of chitosan and water in the scaffolds prepared by freeze-drying, micropores and porosity of different sizes were produced inside the scaffolds after water sublimation (Figure 4). The freeze-dried scaffolds processed with different concentrations of chitosan are like nets woven with ropes of different thicknesses. The low concentration is a loose mesh of holes woven from thinner ropes, while the high concentration is much more like a dense mesh woven from thicker ropes. Hence, higher concentrations of chitosan lyophilized scaffolds can provide greater support to cells due to their compact structure and thicker hole walls [50–52]. These microscopic supporting forces are superimposed to the elastic modulus of the material macroscopically (Figure 3b). Consequently, the chitosan freeze-dried scaffolds give cells an interface environment with different elasticity, meanwhile other conditions keep the same. This differs from conventional hydrogel matrices because the monomer ratio or crosslinking concentration in the hydrogel is changed in order to adjust the stiffness of the hydrogel [53–55].

The experimental results show that the elasticity of the interface material plays an important role in regulating the growth of macrophages, especially the polarization behavior of macrophages. The results of the ELISA show that most cells were mainly polarized to the M1 type on the scaffold, and a few cells were polarized to the M2 type (Figure 9). The original RAW cells were mainly the M0 type, with a round or nearly round shape, while the polarized cells became larger in size and protruded several pseudopodia [56,57]. The process of cell polarization from M0 to M1 and M2 on the scaffold is similar to the physiological process of macrophages when inflammation occurs in vivo. After the material was implanted in vivo, M0 macrophages were chemotactically recruited to the implantation site through the blood circulation [57]. In the early stage of inflammation, cells are classically activated to M1 macrophages, which release various pro-inflammatory factors to kill pathogens, clean up tissue debris at the injury site and promote scar formation [11–13]. In the late stage of inflammation, macrophages are alternately activated to M2 macrophages, which release various anti-inflammatory factors, inhibit the further development of inflammation and promote extracellular matrix reconstruction and tissue regeneration [58–61]. While days 1–3 were in the early stage of inflammation, most cells on the scaffolds expressed the M1 phenotype. In particular, the degree of M1 phenotype polarization first decreased and then increased with the increase in the matrix hardness, while the M2 phenotype polarization first decreased and then increased with the increase in the matrix hardness, and the turning points were all in the 5% group. It has been reported that stiffness similar to that of collagen fibers promotes the M1 phenotype polarization, and the cells appear round. Stiffness similar to that of bone is more favorable for the M2 phenotype polarization, and the cells have a long and spindle-like shape [62]. When the elastic modulus of the Eucommia ulmoides gum (EUG)-based scaffold was reduced to the Mpa level, the RAW 264.7 increased the secretion of inflammatory cytokines which may suggest a different mechanism for macrophages in harder tissues such as articular cartilage [63]. We therefore propose that the polarizing effect of the matrix stiffness on macrophages is biphasic.

The elasticity of the matrix acts as a physical cue through the contact between cells and the matrix. When cells come into contact with the interface, integrin receptors bind to the

material, forming cell–substrate anchor points [64]. Forces are transmitted from the integrin anchored at the cell–substrate sites into the cell, forming focal adhesions (FA) within the cell. Subsequently, the force is transmitted into the cell and alters the arrangement of the cellular actin skeleton through a signaling cascade. The chromatin structure in the nucleus changes accordingly and regulates the expression of genes which eventually changes the shape and function of the cell [65]. Chitosan freeze-dried scaffolds with various concentrations impart different forces to cells. The force that is delivered into cells offers intracellular forces, which are key factors in the regulation of cellular behavior and function by physical cues [66,67]. When the provided force is too small, a firm bond cannot be formed between the cells and the matrix, which reduces the intracellular force and affects the adhesion and proliferation of cells. As the hardness increases, the force provided to the cell elevates, the intracellular force becomes larger, and the function of the cell is improved. In addition to the difference in the elastic modulus, the pore size of freeze-dried scaffolds also affects cells as a topological clue [68]. When the chitosan concentration of the scaffold continues to increase, the pore size of the stent also decreases. The too-small pore size acts as a micropattern and inhibits the extension of the skeleton through spatial constraints and limiting intracellular forces. Thereby, the number and area of the RAW cells decreased in the 7% group as the restriction of the cytoskeletal stretch inhibited cell proliferation and migration (Figure 8).

Macrophages differentiated into different subtypes secrete pro-inflammatory or anti-inflammatory factors, which have profound implications for tissue repair and regeneration [11–13]. The ELISA assay shows that macrophages secreted the M1-type characteristic cytokine IL-6 and the M2-type characteristic cytokine IL-10 (Figure 9). The results of the qPCR also prove that the trend of the M1 phenotype-related gene IL-1 was also consistent with the results of the ELISA (Figure 10). That is to say, in the 1%–5% group, the pro-inflammatory factors secreted by the RAW cells gradually increased, and the anti-inflammatory factors gradually decreased. Conversely, the 5%–7% group showed the opposite trend. From this, we were inspired that the amount of pro- or anti-inflammatory factors secreted by macrophages can be modulated by controlling the stiffness of the freeze-dried scaffolds, thereby reducing the inflammatory response of the biomaterials.

5. Conclusions

In this study, we successfully developed chitosan freeze-dried scaffolds with different elastic modulus to study the effect of matrix elasticity on the behavior and function of macrophages. Through experiments, we found that the 5% concentration of the chitosan scaffold had the best effect on promoting cell proliferation. In addition, the 5% group can maximize the polarization of the macrophages to the M2 phenotype and inhibited the polarization of the macrophages to the M1 phenotype, thereby inhibiting FBR and improving the biocompatibility of the chitosan scaffolds. In addition, we found that the polarization regulation of the macrophages by the matrix stiffness was bidirectional. In the low elastic modulus range, high stiffness promotes the differentiation of macrophages towards the M2 phenotype, whereas in the high elastic modulus range, high stiffness promotes the differentiation of macrophages towards the M1 phenotype. Thus, our study may provide new insights and references for designing the elastic moduli of biomaterials for regulating immune responsiveness.

Author Contributions: Conceptualization, J.X., W.G. and Y.K.; methodology, F.L.; software, J.X.; validation, J.X., Y.K. and W.G.; formal analysis, J.X.; investigation, J.X.; resources, Y.Z.; data curation, J.X.; writing—original draft preparation, J.X.; writing—review and editing, G.L.; visualization, J.X.; supervision, Y.Y.; project administration, Y.Y.; funding acquisition, Y.Y. All authors have read and agreed to the published version of the manuscript.

Funding: The authors gratefully acknowledge the financial support of the National Natural Science Foundation of China (32230057, 32171352), the Open Project of the State Key Laboratory of Polymer Materials Engineering (Sichuan University) (sklpme2022-4-01), the Guangxi Key Laboratory of Regenerative Medicine (Guizaizhongkai202101) and the National Engineering Laboratory for Modern Silk, Soochow University (SDGC2147). 226 High-level Talent Training Project (2ndlevel, 2022).

Institutional Review Board Statement: Not applicable.

Informed Consent Statement: Not applicable.

Data Availability Statement: Not applicable.

Conflicts of Interest: The authors declare no conflict of interest.

References

1. Chen, H.; Agrawal, D.K.; Thankam, F.G. Biomaterials-Driven Sterile Inflammation. *Tissue Eng. Part B-Rev.* **2022**, *28*, 22–34. [[CrossRef](#)] [[PubMed](#)]
2. Wang, Y.J. Bioadaptability: An Innovative Concept for Biomaterials. *J. Mater. Sci. Technol.* **2016**, *32*, 801–809. [[CrossRef](#)]
3. Anderson, J.M.; Rodriguez, A.; Chang, D.T. Foreign body reaction to biomaterials. *Semin. Immunol.* **2008**, *20*, 86–100. [[CrossRef](#)] [[PubMed](#)]
4. Zdolsek, J.; Eaton, J.W.; Tang, L. Histamine release and fibrinogen adsorption mediate acute inflammatory responses to biomaterial implants in humans. *J. Transl. Med.* **2007**, *5*, 31. [[CrossRef](#)]
5. Ibrahim, M.M.; Medina, M.A.; Bond, J.; Chen, L.; Quiles, C.; Kokosis, G.; Bashirov, L.; Selim, A.; Klitzman, B.; Levinson, H. Foreign body reaction to commonly used surgical biomaterials. *Wound Repair Regen.* **2016**, *24*, A12–A13.
6. Zhou, G.Y.; Groth, T. Host Responses to Biomaterials and Anti-Inflammatory Design—A Brief Review. *Macromol. Biosci.* **2018**, *18*, 1800112. [[CrossRef](#)]
7. Wu, Y.L.; Zhang, C.H.; Teng, Y.; Pan, Y.; Liu, N.C.; Liu, P.X.; Zhu, X.; Su, X.L.; Lin, J. Propionate and butyrate attenuate macrophage pyroptosis and osteoclastogenesis induced by CoCrMo alloy particles. *Mil. Med. Res.* **2022**, *9*, 46. [[CrossRef](#)]
8. Klopffleisch, R.; Jung, F. The pathology of the foreign body reaction against biomaterials. *J. Biomed. Mater. Res. Part A* **2017**, *105*, 927–940. [[CrossRef](#)]
9. Abumaree, M.H.; Al Harthy, S.; Al Subayyil, A.M.; Alshabibi, M.A.; Abomaray, F.M.; Khatlani, T.; Kalionis, B.; El-Muzaini, M.F.; Al Jumah, M.A.; Jawdat, D.; et al. Decidua Basalis Mesenchymal Stem Cells Favor Inflammatory M1 Macrophage Differentiation In Vitro. *Cells* **2019**, *8*, 173. [[CrossRef](#)]
10. Veremeyko, T.; Yung, A.W.Y.; Anthony, D.C.; Strelakova, T.; Ponomarev, E.D. Early Growth Response Gene-2 Is Essential for M1 and M2 Macrophage Activation and Plasticity by Modulation of the Transcription Factor CEBPbeta. *Front. Immunol.* **2018**, *9*, 2515. [[CrossRef](#)]
11. Shrivastava, R.; Shukla, N. Attributes of alternatively activated (M2) macrophages. *Life Sci.* **2019**, *224*, 222–231. [[CrossRef](#)]
12. Wang, Q.; He, Z.; Huang, M.; Liu, T.; Wang, Y.; Xu, H.; Duan, H.; Ma, P.; Zhang, L.; Zamvil, S.S.; et al. Vascular niche IL-6 induces alternative macrophage activation in glioblastoma through HIF-2alpha. *Nat. Commun.* **2018**, *9*, 559. [[CrossRef](#)] [[PubMed](#)]
13. Alvarado-Vazquez, P.A.; Bernal, L.; Paige, C.A.; Grosick, R.L.; Moracho Vilrriales, C.; Ferreira, D.W.; Ulecia-Moron, C.; Romero-Sandoval, E.A. Macrophage-specific nanotechnology-driven CD163 overexpression in human macrophages results in an M2 phenotype under inflammatory conditions. *Immunobiology* **2017**, *222*, 900–912. [[CrossRef](#)]
14. Xu, X.W.; Gu, S.C.; Huang, X.; Ren, J.Y.; Gu, Y.H.; Wei, C.J.; Lian, X.; Li, H.Z.; Gao, Y.S.; Jin, R.; et al. The role of macrophages in the formation of hypertrophic scars and keloids. *Burn. Trauma* **2020**, *8*, tkaa006. [[CrossRef](#)] [[PubMed](#)]
15. Bonito, V.; de Kort, B.J.; Bouten, C.V.C.; Smits, A.I.P.M. Cyclic Strain Affects Macrophage Cytokine Secretion and Extracellular Matrix Turnover in Electrospun Scaffolds. *Tissue Eng. Part A* **2019**, *25*, 1310–1325. [[CrossRef](#)] [[PubMed](#)]
16. Di Cio, S.; Gautrot, J.E. Cell sensing of physical properties at the nanoscale: Mechanisms and control of cell adhesion and phenotype. *Acta Biomater.* **2016**, *30*, 26–48. [[CrossRef](#)] [[PubMed](#)]
17. Ye, K.; Cao, L.P.; Li, S.Y.; Yu, L.; Ding, J.D. Interplay of Matrix Stiffness and Cell-Cell Contact in Regulating Differentiation of Stem Cells. *ACS Appl. Mater. Interfaces* **2016**, *8*, 21903–21913. [[CrossRef](#)]
18. Feng, P.; Wu, P.; Gao, C.D.; Yang, Y.W.; Guo, W.; Yang, W.J.; Shuai, C.J. A Multimaterial Scaffold With Tunable Properties: Toward Bone Tissue Repair. *Adv. Sci.* **2018**, *5*, 1700817. [[CrossRef](#)]
19. Fan, D.Y.; Wang, Q.; Zhu, T.J.; Wang, H.F.; Liu, B.C.; Wang, Y.F.; Liu, Z.J.; Liu, X.Y.; Fan, D.W.; Wang, X. Recent Advances of Magnetic Nanomaterials in Bone Tissue Repair. *Front. Chem.* **2020**, *8*, 745. [[CrossRef](#)]
20. Whitehead, A.K.; Barnett, H.H.; Calderera-Moore, M.E.; Newman, J.J. Poly (ethylene glycol) hydrogel elasticity influences human mesenchymal stem cell behavior. *Regen. Biomater.* **2018**, *5*, 167–175. [[CrossRef](#)]
21. Deng, M.; Lin, J.; Nowsheen, S.; Liu, T.Z.; Zhao, Y.C.; Villalta, P.W.; Sicard, D.; Tschumperlin, D.J.; Lee, S.; Kim, J.; et al. Extracellular matrix stiffness determines DNA repair efficiency and cellular sensitivity to genotoxic agents. *Sci. Adv.* **2020**, *6*, eabb2630. [[CrossRef](#)] [[PubMed](#)]

22. Zeng, Y.Y.; Yi, J.Y.; Wan, Z.P.; Liu, K.; Song, P.; Chau, A.; Wang, F.; Chang, Z.; Han, W.D.; Zheng, W.J.; et al. Substrate stiffness regulates B-cell activation, proliferation, class switch, and T-cell-independent antibody responses in vivo. *Eur. J. Immunol.* **2015**, *45*, 1621–1634. [[CrossRef](#)] [[PubMed](#)]
23. Lv, H.W.; Wang, H.P.; Zhang, Z.J.; Yang, W.; Liu, W.B.; Li, Y.L.; Li, L.S. Biomaterial stiffness determines stem cell fate. *Life Sci.* **2017**, *178*, 42–48. [[CrossRef](#)] [[PubMed](#)]
24. Oh, S.H.; An, D.B.; Kim, T.H.; Lee, J.H. Wide-range stiffness gradient PVA/HA hydrogel to investigate stem cell differentiation behavior. *Acta Biomater.* **2016**, *35*, 23–31. [[CrossRef](#)] [[PubMed](#)]
25. He, X.T.; Wu, R.X.; Xu, X.Y.; Wang, J.; Yin, Y.; Chen, F.M. Macrophage involvement affects matrix stiffness-related influences on cell osteogenesis under three-dimensional culture conditions. *Acta Biomater.* **2018**, *71*, 132–147. [[CrossRef](#)] [[PubMed](#)]
26. Adlerz, K.M.; Aranda-Espinoza, H.; Hayenga, H.N. Substrate elasticity regulates the behavior of human monocyte-derived macrophages. *Eur. Biophys. J. Biophys. Lett.* **2016**, *45*, 301–309. [[CrossRef](#)]
27. Lee, A.; Septiadi, D.; Taladriz-Blanco, P.; Almeida, M.; Haeni, L.; Spuch-Calvar, M.; Abdussalam, W.; Rothen-Rutishauser, B.; Petri-Fink, A. Particle Stiffness and Surface Topography Determine Macrophage-Mediated Removal of Surface Adsorbed Particles. *Adv. Healthc. Mater.* **2021**, *10*, 2001667. [[CrossRef](#)]
28. Seidlits, S.K.; Khaing, Z.Z.; Petersen, R.R.; Nickels, J.D.; Vanscoy, J.E.; Shear, J.B.; Schmidt, C.E. The effects of hyaluronic acid hydrogels with tunable mechanical properties on neural progenitor cell differentiation. *Biomaterials* **2010**, *31*, 3930–3940. [[CrossRef](#)]
29. Zhao, X.H. Multi-scale multi-mechanism design of tough hydrogels: Building dissipation into stretchy networks. *Soft Matter* **2014**, *10*, 672–687. [[CrossRef](#)]
30. Denisin, A.K.; Pruitt, B.L. Tuning the Range of Polyacrylamide Gel Stiffness for Mechanobiology Applications. *ACS Appl. Mater. Interfaces* **2016**, *8*, 21893–21902. [[CrossRef](#)]
31. Munteanu, B.S.; Paslaru, E.; Zemljic, L.F.; Sdrobis, A.; Pricope, G.M.; Vasile, C. Chitosan Coatings Applied to Polyethylene Surface to Obtain Food-Packaging Materials. *Cellul. Chem. Technol.* **2014**, *48*, 565–575.
32. Negm, N.A.; Hefni, H.H.H.; Abd-Elaal, A.A.A.; Badr, E.A.; Abou Kana, M.T.H. Advancement on modification of chitosan biopolymer and its potential applications. *Int. J. Biol. Macromol.* **2020**, *152*, 681–702. [[CrossRef](#)] [[PubMed](#)]
33. Liu, X.; Ma, L.; Mao, Z.W.; Gao, C.Y. Chitosan-Based Biomaterials for Tissue Repair and Regeneration. In *Chitosan for Biomaterials II*; Jayakumar, R., Prabakaran, M., Muzzarelli, R.A.A., Eds.; Advances in Polymer Science; Springer: Berlin/Heidelberg, Germany, 2011; Volume 244, pp. 81–127.
34. Li, J.H.; Zhuang, S.L. Antibacterial activity of chitosan and its derivatives and their interaction mechanism with bacteria: Current state and perspectives. *Eur. Polym. J.* **2020**, *138*, 109984. [[CrossRef](#)]
35. Kong, Y.; Tang, X.X.; Zhao, Y.H.; Chen, X.L.; Yao, K.; Zhang, L.L.; Han, Q.; Zhang, L.Z.; Ling, J.; Wang, Y.J.; et al. Degradable tough chitosan dressing for skin wound recovery. *Nanotechnol. Rev.* **2020**, *9*, 1576–1585. [[CrossRef](#)]
36. Li, G.C.; Xiao, Q.Z.; Zhang, L.Z.; Zhao, Y.H.; Yang, Y.M. Nerve growth factor loaded heparin/chitosan scaffolds for accelerating peripheral nerve regeneration. *Carbohydr. Polym.* **2017**, *171*, 39–49. [[CrossRef](#)] [[PubMed](#)]
37. Li, G.C.; Zhao, X.Y.; Zhang, L.Z.; Wang, C.P.; Shi, Y.W.; Yang, Y.M. Regulating Schwann Cells Growth by Chitosan Micropatterning for Peripheral Nerve Regeneration In Vitro. *Macromol. Biosci.* **2014**, *14*, 1067–1075. [[CrossRef](#)]
38. Li, G.C.; Zhao, X.Y.; Zhao, W.X.; Zhang, L.Z.; Wang, C.P.; Jiang, M.R.; Gu, X.S.; Yang, Y.M. Porous chitosan scaffolds with surface micropatterning and inner porosity and their effects on Schwann cells. *Biomaterials* **2014**, *35*, 8503–8513. [[CrossRef](#)]
39. Zhang, L.Z.; Dou, S.F.; Li, Y.; Yuan, Y.; Ji, Y.W.; Wang, Y.L.; Yang, Y.M. Degradation and compatibility behaviors of poly(glycolic acid) grafted chitosan. *Mater. Sci. Eng. C-Mater. Biol. Appl.* **2013**, *33*, 2626–2631. [[CrossRef](#)]
40. Genasan, K.; Mehrali, M.; Veerappan, T.; Talebian, S.; Raman, M.M.; Singh, S.; Swamiappan, S.; Mehrali, M.; Kamarul, T.; Raghavendran, H.R.B. Calcium-Silicate-Incorporated Gellan-Chitosan Induced Osteogenic Differentiation in Mesenchymal Stromal Cells. *Polymers* **2021**, *13*, 3211. [[CrossRef](#)]
41. Hasany, M.; Talebian, S.; Sadat, S.; Ranjbar, N.; Mehrali, M.; Wallace, G.G.; Mehrali, M. Synthesis, properties, and biomedical applications of alginate methacrylate (ALMA)-based hydrogels: Current advances and challenges. *Appl. Mater. Today* **2021**, *24*, 101150. [[CrossRef](#)]
42. Sacco, P.; Cok, M.; Asaro, F.; Paoletti, S.; Donati, I. The role played by the molecular weight and acetylation degree in modulating the stiffness and elasticity of chitosan gels. *Carbohydr. Polym.* **2018**, *196*, 405–413. [[CrossRef](#)] [[PubMed](#)]
43. Huang, T.T.; Zhou, Z.H.; Li, Q.Y.; Tang, X.X.; Chen, X.L.; Ge, Y.F.; Ling, J. Light-Triggered Adhesive Silk-Based Film for Effective Photodynamic Antibacterial Therapy and Rapid Hemostasis. *Front. Bioeng. Biotechnol.* **2022**, *9*, 820434. [[CrossRef](#)] [[PubMed](#)]
44. Tang, X.X.; Chen, X.L.; Zhang, S.M.; Gu, X.Y.; Wu, R.H.; Huang, T.T.; Zhou, Z.H.; Sun, C.; Ling, J.; Liu, M.; et al. Silk-Inspired In Situ Hydrogel with Anti-Tumor Immunity Enhanced Photodynamic Therapy for Melanoma and Infected Wound Healing. *Adv. Funct. Mater.* **2021**, *31*, 2101320. [[CrossRef](#)]
45. Li, G.C.; Li, S.J.; Zhang, L.L.; Chen, S.Y.; Sun, Z.D.; Li, S.Q.; Zhang, L.Z.; Yang, Y.M. Construction of Biofunctionalized Anisotropic Hydrogel Micropatterns and Their Effect on Schwann Cell Behavior in Peripheral Nerve Regeneration. *ACS Appl. Mater. Interfaces* **2019**, *11*, 37397–37410. [[CrossRef](#)] [[PubMed](#)]
46. Chen, Y.; Zhang, X. Pivotal regulators of tissue homeostasis and cancer: Macrophages. *Exp. Hematol. Oncol.* **2017**, *6*, 23. [[CrossRef](#)]
47. Zhou, H.Q.; Xue, Y.Z.B.; Dong, L.; Wang, C.M. Biomaterial-based physical regulation of macrophage behaviour. *J. Mater. Chem. B* **2021**, *9*, 3608–3621. [[CrossRef](#)] [[PubMed](#)]

48. Evans, N.D.; Gentleman, E. The role of material structure and mechanical properties in cell-matrix interactions. *J. Mater. Chem. B* **2014**, *2*, 2345–2356. [[CrossRef](#)]
49. Kong, Y.; Wang, D.; Wei, Q.F.; Yang, Y.M. Nerve Decellularized Matrix Composite Scaffold with High Antibacterial Activity for Nerve Regeneration. *Front. Bioeng. Biotechnol.* **2022**, *9*, 840421. [[CrossRef](#)]
50. Kumar, A.; Negi, Y.S.; Choudhary, V.; Bhardwaj, N.K.; Han, S.S. Morphological, mechanical, and in vitro cytocompatibility analysis of poly(vinyl alcohol)-silica glass hybrid scaffolds reinforced with cellulose nanocrystals. *Int. J. Polym. Anal. Charact.* **2017**, *22*, 139–151. [[CrossRef](#)]
51. Kumar, A.; Negi, Y.S.; Choudhary, V.; Bhardwaj, N.K. Fabrication of poly (vinyl alcohol)/ovalbumin/cellulose nanocrystals/nanohydroxyapatite based biocomposite scaffolds. *Int. J. Polym. Mater. Polym. Biomater.* **2016**, *65*, 191–201. [[CrossRef](#)]
52. Offeddu, G.S.; Ashworth, J.C.; Cameron, R.E.; Oyen, M.L. Multi-scale mechanical response of freeze-dried collagen scaffolds for tissue engineering applications. *J. Mech. Behav. Biomed. Mater.* **2015**, *42*, 19–25. [[CrossRef](#)] [[PubMed](#)]
53. Chen, S.; Shi, J.; Xu, X.; Ding, J.; Zhong, W.; Zhang, L.; Xing, M.; Zhang, L. Study of stiffness effects of poly(amidoamine)-poly(n-isopropyl acrylamide) hydrogel on wound healing. *Colloids Surf. B-Biointerfaces* **2016**, *140*, 574–582. [[CrossRef](#)] [[PubMed](#)]
54. Fadeev, M.; Davidson-Rozenfeld, G.; Biniuri, Y.; Yakobi, R.; Cazelles, R.; Aleman-Garcia, M.A.; Willner, I. Redox-triggered hydrogels revealing switchable stiffness properties and shape-memory functions. *Polym. Chem.* **2018**, *9*, 2905–2912. [[CrossRef](#)]
55. Wang, C.; Liu, X.; Wulf, V.; Vazquez-Gonzalez, M.; Fadeev, M.; Willner, I. DNA-Based Hydrogels Loaded with Au Nanoparticles or Au Nanorods: Thermoresponsive Plasmonic Matrices for Shape-Memory, Self-Healing, Controlled Release, and Mechanical Applications. *ACS Nano* **2019**, *13*, 3424–3433. [[CrossRef](#)]
56. Sun, Y.L.; Kuang, Y.Y.; Zuo, Z.; Zhang, J.; Ma, X.L.; Xing, X.Y.; Liu, L.Y.; Miao, Y.C.; Ren, T.; Li, H.; et al. Cellular processes involved in RAW 264.7 macrophages exposed to NPFF: A transcriptional study. *Peptides* **2021**, *136*, 170469. [[CrossRef](#)] [[PubMed](#)]
57. Shapouri-Moghaddam, A.; Mohammadian, S.; Vazini, H.; Taghadosi, M.; Esmaeili, S.A.; Mardani, F.; Seifi, B.; Mohammadi, A.; Afshari, J.T.; Sahebkar, A. Macrophage plasticity, polarization, and function in health and disease. *J. Cell. Physiol.* **2018**, *233*, 6425–6440. [[CrossRef](#)] [[PubMed](#)]
58. Baptista, D.; Teixeira, L.; van Blitterswijk, C.; Giselbrecht, S.; Truckenmuller, R. Overlooked? Underestimated? Effects of Substrate Curvature on Cell Behavior. *Trends Biotechnol.* **2019**, *37*, 838–854. [[CrossRef](#)]
59. Barbucci, R.; Lamponi, S.; Borzacchiello, A.; Ambrosio, L.; Fini, M.; Torricelli, P.; Giardino, R. Hyaluronic acid hydrogel in the treatment of osteoarthritis. *Biomaterials* **2002**, *23*, 4503–4513. [[CrossRef](#)]
60. Barth, K.A.; Waterfield, J.D.; Brunette, D.M. The effect of surface roughness on RAW 264.7 macrophage phenotype. *J. Biomed. Mater. Res. Part A* **2013**, *101*, 2679–2688. [[CrossRef](#)]
61. Martin-Cofreces, N.B.; Sanchez-Madrid, F. Sailing to and Docking at the immune Synapse: Role of Tubulin Dynamics and Molecular Motors. *Front. Immunol.* **2018**, *9*, 1174. [[CrossRef](#)]
62. Hersel, U.; Dahmen, C.; Kessler, H. RGD modified polymers: Biomaterials for stimulated cell adhesion and beyond. *Biomaterials* **2003**, *24*, 4385–4415. [[CrossRef](#)]
63. Jansen, L.E.; Amer, L.D.; Chen, E.Y.T.; Nguyen, T.V.; Saleh, L.S.; Emrick, T.; Liu, W.F.; Bryant, S.J.; Peyton, S.R. Zwitterionic PEG-PC Hydrogels Modulate the Foreign Body Response in a Modulus-Dependent Manner. *Biomacromolecules* **2018**, *19*, 2880–2888. [[CrossRef](#)] [[PubMed](#)]
64. Sit, S.T.; Manser, E. Rho GTPases and their role in organizing the actin cytoskeleton. *J. Cell Sci.* **2011**, *124*, 679–683. [[CrossRef](#)] [[PubMed](#)]
65. Hou, Y.; Xie, W.Y.; Yu, L.X.; Camacho, L.C.; Nie, C.X.; Zhang, M.; Haag, R.; Wei, Q. Surface Roughness Gradients Reveal Topography-Specific Mechanosensitive Responses in Human Mesenchymal Stem Cells. *Small* **2020**, *16*, 1905422. [[CrossRef](#)]
66. Yanakieva, I.; Erzberger, A.; Matejic, M.; Modes, C.D.; Norden, C. Cell and tissue morphology determine actin-dependent nuclear migration mechanisms in neuroepithelia. *J. Cell Biol.* **2019**, *218*, 3272–3289. [[CrossRef](#)]
67. Yao, X.; Peng, R.; Ding, J.D. Cell-Material Interactions Revealed Via Material Techniques of Surface Patterning. *Adv. Mater.* **2013**, *25*, 5257–5286. [[CrossRef](#)]
68. Liu, W.; Sun, Q.; Zheng, Z.L.; Gao, Y.T.; Zhu, G.Y.; Wei, Q.; Xu, J.Z.; Li, Z.M.; Zhao, C.S. Topographic Cues Guiding Cell Polarization via Distinct Cellular Mechanosensing Pathways. *Small* **2022**, *18*, 2104328. [[CrossRef](#)]